P-ISSN : 2598-1277
E-ISSN : 2621-3966

JOURNAL OF GREEN SCIENCE AND TECHNOLOGY

OPTIMIZATION OF MIXING CHAMBER DESIGN ON STEAM EJECTOR AT GEOTHERMAL POWER PLANT BASED ON CFD SIMULATION

S. S. Rusdan[1] and Y. Suprianti[1*]

[1*)] *Energy Conversion Engineering Department, Politeknik Negeri Bandung 40559*
Corresponding Author's Email: yanti.suprianti@polban.ac.id
No. HP Corresponding Author: (+62)85624890083

ABSTRACT

The initial generation capacity of 30 MW at the Geothermal Power Plant (GPP) decreased to 11.88 MW due to reduced steam supply from production wells. This mismatch between the original system design and current operating conditions affected components such as the steam ejector, which experienced a reduction in motive steam flow from 1.96 kg/s to 1.66 kg/s. As a result, the mixing chamber became inefficient in entraining flow of non- condensable gases (NCG), causing suboptimal pressure ratios (P3/P5), turbulence, and backflow. This study aims to redesign the mixing chamber of the steam ejector to enhance the extraction NCG. Using compressible flow theory and CFD simulation with Ansys Fluent 2025R1, the redesigned geometry improved the entrainment ratio from 0.27 to 0.31 and increased the NCG suction rate from 0.45 kg/s to 0.52 kg/s. The pressure ratio P3/P5 rose from 0.04 to 0.07, approaching optimal conditions. Further analysis revealed that under increased motive flow (1.687 kg/s), the ejector achieved an entrainment ratio of 0.32, and under lowered condenser pressure (8.1 kPa), the entrainment reached 0.34. These two optimal conditions demonstrate the redesigned chamber's adaptability under varied operational scenarios. The performance improvement contributed to an additional power output of 41.68 kWh, approaching the plant's installed capacity and improving system reliability. From economic perspective, the optimization is also feasible, yielding a net present value (NPV) of Rp6.46 million and demonstrating high profitability and practical applicability.

Keywords: NCG, Steam ejector, Mixing chamber, Entrainment ratio, CFD

1. INTRODUCTION

Geothermal power plants (GPP) rely on condenser vacuum to enhance turbine efficiency. However, the presence of non-condensable gases (NCG), such as CO_2 and H_2S, increases condenser pressure and reduces turbine performance, ultimately lowering power output [1], [2]. The steam ejector's performance largely depends on its internal components, especially the mixing chamber where motive steam and NCG interact. An imbalance in design particularly in chamber dimensions can lead to turbulence, energy losses, and backflow, especially under fluctuating gas composition and operating pressures [3].

At PLTP X, the installed generation capacity of 30 MW has decreased to 11.88 MW due to limited steam supply. The motive steam flow rate dropped from 1.96 kg/s to 1.66 kg/s, while NCG suction decreased from 1.3 kg/s to 0.31 kg/s. Additionally, the motive steam pressure declined from 650 kPa (design) to 420 kPa [4].

Recent studies have explored the influence of geometry on ejector performance through computational fluid dynamics (CFD) analysis [5], application of Fano flow models for chamber optimization [6], and evaluation of mixing chamber length in two-phase ejectors [7]. While these studies provide important insights into design improvement, they primarily focus on general or multiphase applications and lack

P-ISSN : 2598-1277
E-ISSN : 2621-3966

real field operational data.

This study aims to evaluate the limitations of the current steam ejector at PLTP X and redesign the mixing chamber geometry to improve entrainment ratio and suction capacity under actual operating conditions. By integrating compressible flow theory and CFD simulation with real plant data, this research offers a field-applicable solution to optimize steam ejector performance in geothermal environments.

2. RESEARCH METHODOLOGY

To provide a structured overview of the research steps, a simplified flowchart is presented below. This diagram outlines the key stages involved in identifying the performance limitations of the current steam ejector, modifying the geometry, evaluating its impact on entrainment ratio, and finalizing the optimized design. Each step incorporates engineering principles, simulation results, and economic considerations to ensure technical feasibility and field applicability.

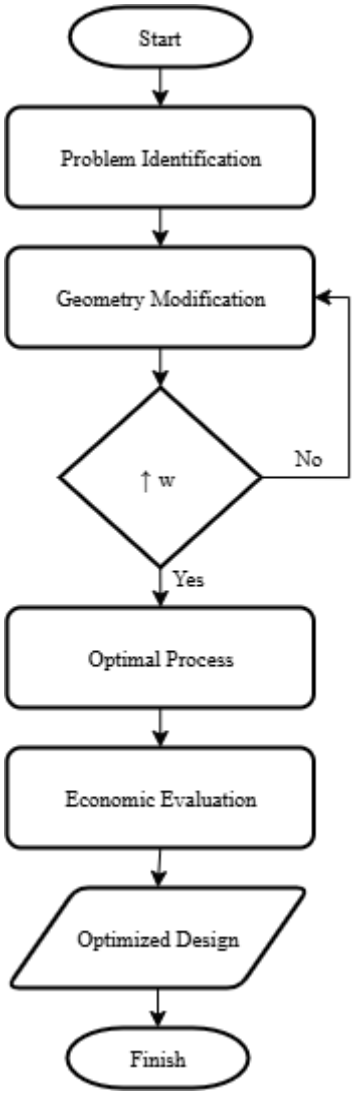

Figure 1. Flowchart Diagram of Optimization Procedure

As illustrated in the Figure 1, the optimization process begins with identifying problems under current field conditions, followed by geometry modification of the mixing chamber. The effectiveness of each design iteration is evaluated based on its ability to increase the entrainment ratio (w). If the performance criteria are met, the process proceeds to operational optimization and economic analysis to determine viability. The final outcome is an optimized ejector design that improves NCG suction

P-ISSN : 2598-1277
E-ISSN : 2621-3966

capacity and supports overall plant efficiency.

2.1 System Data and Initial Assumption

This study is based on operational data from a geothermal power plant referred to as PLTP X. The steam ejector is responsible for extracting non-condensable gases (NCG) from the condenser to maintain vacuum conditions and ensure optimal turbine performance. To analyze and redesign the ejector effectively, it is necessary to define the working fluid characteristics and boundary conditions that reflect current plant conditions.

Figure 1 illustrates the schematic layout of the steam ejector, which consists of five main sections. Motive steam enters through the nozzle (point 1), expands through the nozzle throat (point 2), and mixes with suction gas entering from the side (point 3). The combined flow continues through the mixing chamber and is recompressed in the diffuser section (point 4), then exits toward the inter-condenser (point 5).

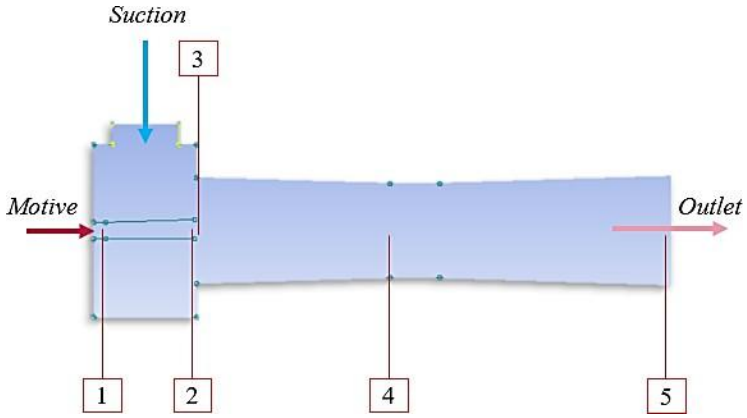

Figure 2. Schematic Diagram

The motive steam is composed of 96% water vapor (H_2O) and 4% carbon dioxide (CO_2), while the suction gas is assumed to be 100% CO_2. The motive flow enters the ejector at a pressure of 420 kPa, temperature of 434 K, and mass flow rate of 1.66 kg/s. The suction pressure is assumed to be equal to the condenser pressure of 8.5 kPa. The outlet pressure at point 5 is set at 19.6 kPa, based on the inter-condenser operating limit. These values form the basis for manual calculation and CFD simulation in the following sections.

2.2 Mixing Chamber Design

Following the identification of suction inefficiency under actual operating conditions, the redesign focuses on adjusting the cross-sectional area of the mixing chamber (A_3). The objective is to increase the pressure ratio between points P_3 and P_5, which serves as an indicator of the chamber's mixing and recompression performance.

The initial geometry of the steam ejector is based on the actual configuration of PLTP X, as shown in Table 1. Among the various sections, the area A_3 is selected as the key optimization target due to its direct influence on entrainment dynamics and pressure recovery.

Table 1. Steam Ejector Geometry

Cross-Sectional Area (m^2)		Length (m)	
Am	1,77 x 10^{-2}	Lm	-
As	2,83 x 10^{-1}	Ls	-
A1	1,77 x 10^{-3}	L1	0,09
A2	4,90 x 10^{-2}	L2	0,87
A3	5,93 x 10^{-2}	L3	1,73
A4	5,41 x 10^{-2}	L4	0,79
A5	1,22 x 10^{-1}	L5	2,76

Source: Internal Operational Report. 2024

P-ISSN : 2598-1277
E-ISSN : 2621-3966

Figure 3 presents the correlation between cross-section area of mixing chamber (A_3) and the pressure ratio P_3/P_5 based on a series of calculation by varying A_3. The graph shows that as A_3 decreases, the pressure ratio increases, approaching the theoretical ideal range of 0.1 to 0.2 [8]. The optimal point is selected at A_3 0.0593 m², which is near the throat area limit, ensuring sufficient flow while minimizing pressure loss.

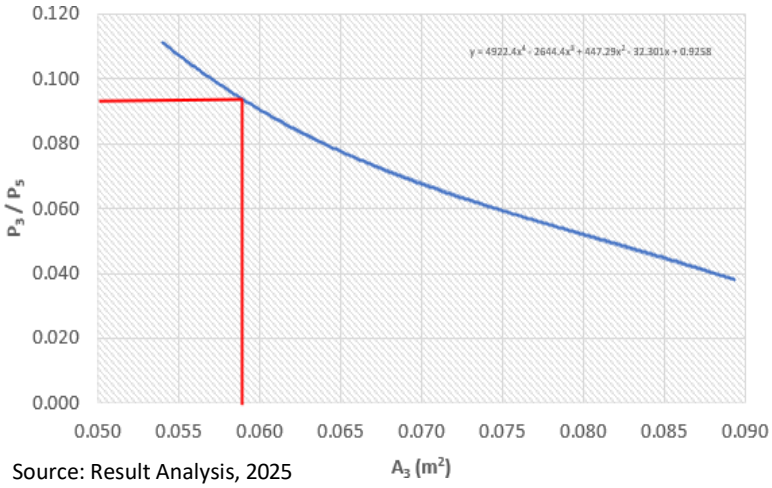

Source: Result Analysis, 2025

Figure 3. Determination of A_3 Based on P_3/P_5 ratio

The design approach follows compressible flow principles under ideal gas assumptions. It considers choked flow at the nozzle throat (Mach 1) and supersonic expansion up to Mach 3 at the outlet. The resulting geometry is used as the input for CFD simulation in the next section.

2.3 CFD Simulation

2.3.1 Determination of Boundary Parameters

Boundary parameters in the CFD simulation were determined based on preliminary calculations using compressible gas flow theory. The objective is to estimate pressure and Mach number at key locations within the ejector system to ensure realistic, physics-based boundary conditions. The following equations are adapted from established compressible flow models.

- Pressure at point 1 (P_1)

$$P_1 = P_m \left(1 + \frac{\gamma - 1}{2} M_1^2\right)^{-\frac{\gamma}{\gamma - 1}} \quad (1)$$

Where: P_m = Motive steam inlet pressure (kPa)

γ = Ratio of specific heats (Cp/Cv)

M_1 = Mach Number of fluid at nozzle throat (assumed chocked, M = 1)

Source: J.D. Anderson 2003

- Pressure at point 2 (P_2)

$$P_2 = P_m \left(\frac{A_1}{A_3}\right)^{\gamma} \left[1 + \frac{\gamma - 1}{2} M_1^2 \left(1 - \left(\frac{A_1}{A_3}\right)^{\gamma}\right)\right]^{-\frac{\gamma}{\gamma - 1}} \quad (2)$$

Where: P_m = Motive steam inlet pressure (kPa)

A_1 = Cross-sectional area at nozzle throat (m2)

A_3 = Cross-sectional area at mixing chamber (m2)

γ = Ratio of specific heats (Cp/Cv)

M_1 = Mach Number of fluid at nozzle throat (assumed chocked, M = 1)

Source: Cengel, Y. A., & Boles, M. A. 2015

P-ISSN : 2598-1277
E-ISSN : 2621-3966

- Pressure at point 3 (P_3)

$$P_3 = P_2 \left(\frac{A_2}{A_3}\right)^{\gamma} \quad (3)$$

Where: P_2 = Pressure at poin 2 (kPa)
A_2 = Cross-sectional area at outlet throat (m2)
A_3 = Cross-sectional area at mixing chamber (m2)
γ = Ratio of specific heats (Cp/Cv)

Source: J.D. Anderson 2003

- Pressure at point 4 (P_4)

$$P_4 = P_3 \left(\frac{A_3}{A_4}\right)^{\gamma} e^{\left(-f\,\theta_3 \frac{L_3}{D_3}\right)} \quad (4)$$

Where: P_3 = Pressure at poin 3 (kPa)
A_3 = Cross-sectional area at mixing chamber (m2)
A_4 = Cross-sectional area at throat (m2)
γ = Ratio of specific heats (Cp/Cv)
e = Navier Factor (2,718)
f = Factor friction
θ_3 = Convergence angle of mixing chamber
L_3 = Horizontal length of mixing chamber (m)
D_3 = Cross-sectional diameter (m)

Source: J.D. Anderson 2003

- Mach Number of motive fluid at nozzle outlet (M_{m2})

$$M_{m2} = \sqrt{\left(\frac{2\eta_n}{\gamma - 1}\right)\left[\left(\frac{P_m}{P_2}\right)^{\frac{\gamma-1}{\gamma}} - 1\right]} \quad (5)$$

Where: η_n = Nozzle efficiency (%)
γ = Ratio of specific heats (Cp/Cv)
P_m = Motive steam inlet pressure (kPa)
P_2 = Pressure at poin 2 (kPa)

Source: H. El-Dessouky et al. 2002

- Mach Number of suction fluid at nozzle outlet (M_{s2})

$$M_{s2} = \sqrt{\left(\frac{2}{\gamma - 1}\right)\left[\left(\frac{P_s}{P_2}\right)^{\frac{\gamma-1}{\gamma}} - 1\right]} \quad (6)$$

Where: γ = Ratio of specific heats (Cp/Cv)
P_s = suction inlet pressure (kPa)
P_2 = Pressure at poin 2 (kPa)

Source: H. El-Dessouky et al. 2002

P-ISSN : 2598-1277
E-ISSN : 2621-3966

- Critical Mach Number at point 4 (M_4*)

$$M_4^* = \frac{M_{m2}^* + w\, M_{s2}^* \sqrt{\frac{T_s}{T_m}}}{\sqrt{(1+w)\left(1+w\frac{T_s}{T_m}\right)}} \quad (7)$$

Where: M_4* = Critical Mach Number at point 4
M_{m2}* = Critical Mach Number motive fluid at point 2
M_{s2}* = Critical Mach Number suction fluid at point 2
w = Entrainment ration (assumed from actual data)
T_s = Temperature of suction fluid
T_m = Temperature of motive fluid

Source: H. El-Dessouky et al. 2002

- M* used to find: M_{s2}*, M_{m2}*, dan M_4

$$M^* = \sqrt{\frac{M^2(\gamma+1)}{M^2(\gamma-1)+2}} \quad (8)$$

Where: M* = Critical Mach Number "Z"
M = Mach Number at point "Z"
γ = Ratio of specific heats (Cp/Cv)

Source: H. El-Dessouky et al. 2002

- Mach Number at point 4' (M_4')

$$M_{4'} = \frac{{M_4}^2 + \frac{2}{(\gamma-1)}}{\frac{2}{(\gamma-1)}{M_4}^2 - 1} \quad (9)$$

Where: M_4' = Mach Number at poin 4' (after shockwave)
M_4 = Mach Number at point 4
γ = Ratio of specific heats (Cp/Cv)

Source: H. El-Dessouky et al. 2002

- Pressure after shockwave at point 4' (P_4')

$$\frac{P_{4'}}{P_4} = \frac{1+\gamma M_4^2}{1+\gamma M_{4'}^2} \quad (10)$$

Where: P4 = Pressure at point 4 (kPa)
γ = Ratio of specific heats (Cp/Cv)
M_4' = Mach Number at point 4' (after shockwave)
M_4 = Mach Number at point 4

Source: H. El-Dessouky et al. 2002

- Pressure lift at diffuser (P_5)

$$\frac{P_5}{P_{4'}} = \left[\frac{\eta_d(\gamma-1)\, M_{4'}^2}{2} + 1\right]^{\frac{\gamma}{\gamma-1}} \quad (11)$$

P-ISSN : 2598-1277
E-ISSN : 2621-3966

Where: P_4' = Pressure at point 4' (kPa)

η_d = Diffuser eficiency (%)

γ = Ratio of specific heats (Cp/Cv)

M_4' = Mach Number at poin 4' (after shockwave)

Source: H. El-Dessouky et al. 2002

The overall workflow begins with theoretical calculations using Equations (1) through (11) to estimate static pressures and Mach numbers at critical points within the ejector system. These calculations provide an initial estimate of the outlet pressure (P_5), which is used as a target boundary condition in the CFD simulation. Subsequently, Equation (12) is used to convert static pressures and Mach numbers into total (gauge) pressures for the motive and suction inlets, as required by the CFD software.

After running the CFD simulation with these boundary conditions, the resulting mass flow rates of suction and motive fluids are extracted. From these values, the entrainment ratio (w) is determined. This new ratio is then fed back into the analytical process, particularly into Equations (7) and (11), to recalculate the critical Mach number and outlet pressure (P_5). The goal is to refine the calculation until the results converge and reflect consistent flow behavior between theory and simulation.

2.3.2 *Setup* Model CFD

The simulation was performed using Ansys Fluent 2025R1 with a designed geometry. The domain was modeled in 3D and generated approximately 996,000 cells, with skewness values ranging from 0.3 to 0.6. A pressure-based solver was applied with the SST k-omega turbulence model, along with activation of energy and species transport models to simulate the steam and CO_2 mixture [9].

Boundary conditions included a mass flow inlet for the motive flow (containing 96% H_2O and 4% CO_2), a pressure inlet for the suction flow (containing 100% of CO_2), and a pressure outlet as defined by the previous pressure boundary calculation (P_5) in Subsection 2.3.1. The initial gauge pressures at both motive and suction inlets were calculated based on the pressure ratio equation for compressible gas flow [10].

$$\frac{P_t}{P} = \left(1 + \frac{\gamma - 1}{2} M^2\right)^{\frac{\gamma}{\gamma - 1}} \quad (12)$$

Where: P_t = Initial gauge pressure/supersonic (kPa)

P = Pressure motive or suction (kPa)

M = Mach Number at point 2 of motive or suction

γ = Ratio of specific heats (C_p/C_v)

Source: J.D. Anderson 2003

The fluid properties were set as ideal gas with specific heat capacity (C_p) defined using a piecewise polynomial function. The numerical scheme applied was SIMPLEC, with second-order upwind for pressure, momentum, and density, and first-order upwind for energy and species. The simulation was run for up to 2,500 iterations, and convergence residual threshold of one thousandth.

2.3.3 Evaluation Parameters

The ejector performance evaluation focused on the key parameter, the entrainment ratio. The outlet pressure (P_5) was determined manually using the compressible flow equations (1) through (11), while the initial gauge pressures at the motive and suction inlets were calculated using equation (12). The CFD simulation results were then used to obtain the entrainment ratio as the main indicator reflecting of the success of the mixing chamber design optimization.

P-ISSN : 2598-1277
E-ISSN : 2621-3966

3. RESULT AND DISCUSSION

3.1 Initial Model Validation

To ensure that the CFD model accurately represents the actual operating conditions of the steam ejector, a validation step was performed by comparing key process parameters derived from the theoretical calculations (Equations 1 through 11) with actual field data. Table 2 presents the main parameters at significant ejector points, including pressure values and derived Mach numbers used in the simulation.

Table 2. Process Parameters

Parameter	Actual	Design
P_1	227.87 kPa	227.87 kPa
P_2	2.18 kPa	3.76 kPa
P_3	1.00 kPa	2.93 kPa
P_4	1.92 kPa	3.31 kPa
$P_{4'}$	23.78 kPa	30.82 kPa
P_5	24.36 kPa	31.81 kPa

As shown in Table 2, the design condition represents an improved ejector configuration compared to the actual operating data. The pressure ratio between point 3 and point 5 (P_3/P_5) increases from 0.04 to 0.09, while the entrainment ratio also improves from 0.27 to 0.31 based on the CFD simulation. These trends indicate enhanced suction performance and support the validity of the simulation model. Consequently, the model is considered suitable for further design evaluation and optimization in the following sections.

3.2 Pressure Distribution

The pressure distribution from the CFD simulation is presented in Figure 4. The absolute pressure values were obtained by adding the atmospheric pressure of 86,600 Pa to the gauge pressure results from the simulation. The recorded values include pressure at point P1 of 187.30 kPa, P2 at 1.73 kPa, P3 at 2.38 kPa, P4 at 5.71 kPa, P4′ at 20.32 kPa, and P5 at 26.59 kPa.

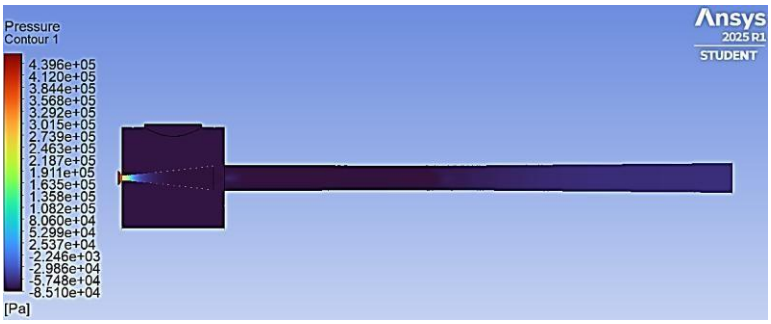

Figure 4. Pressure Distribution

A comparison between the simulation results and theoretical design values reveals varying degrees of deviation at each point. The largest error occurs at point P_4, with a deviation of 72%, likely due to turbulence and shockwave effects that are not fully accounted for in one-dimensional theoretical calculations. Other deviations include 54% at P_2, 34% at $P_{4'}$, 19% at P_3, 18% at P_1, and the lowest error of 16% at P_5. Despite these differences, the pressure profile shows a consistent trend that validates the simulation's predictive capability.

The visual distribution in Figure 4 highlights a high-pressure zone at the diffuser inlet and a shockwave formation near the throat area, indicated by a sudden pressure rise and color shift. This confirms the transition from supersonic to subsonic flow, a phenomenon expected in ejector performance under compressible conditions. The simulation supports the achievement of an entrainment ratio of 0.31,

P-ISSN : 2598-1277
E-ISSN : 2621-3966

indicating improved suction performance compared to the actual operating condition.

3.3 Impact of Geometry Modification

Figure 5 shows the velocity vector distribution illustrating the interaction between the motive steam and non-condensable gas (NCG) within the mixing chamber. The high-velocity motive steam is seen entering from the left and forming a uniform jet that gradually entrains the suction flow. The flow remains aligned predominantly in the downstream direction, especially near the mixing chamber walls, indicating a reduction in reverse flow and turbulence. This behavior confirms that the modified geometry successfully supports stable and efficient mixing.

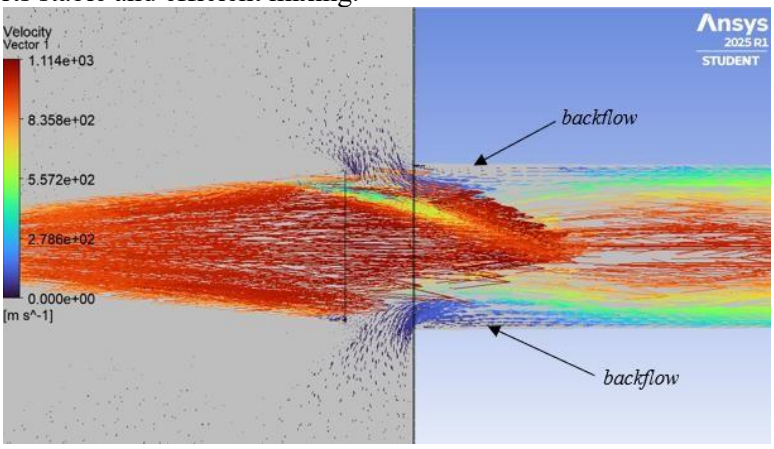

Figure 5. Velocity Vector Distribution within The Mixing Chamber

The geometric adjustment—specifically the reduction of the mixing chamber cross-sectional area (A_3)—has a direct impact on ejector performance. The entrainment ratio increases from 0.27 to 0.31, while the NCG suction mass flow improves from 0.45 kg/s to 0.52 kg/s. In addition, the pressure ratio between points P_3 and P_5 rises from 0.04 to 0.07, moving closer to the ideal range for effective compressible gas mixing. These improvements demonstrate that the optimized chamber dimensions contribute significantly to enhancing the ejector's suction capability and overall system stability under actual operating conditions.

3.4 Energy Implication for System

The improved performance of the steam ejector has a direct effect on the power plant's energy output. According to A. Horas et al. [2], 1% increase in non-condensable gas (NCG) concentration in the condenser can reduce power output by up to 1.6%. In this study, the suction capacity of the ejector increased from 0.45 kg/s to 0.52 kg/s, indicating a reduction in NCG accumulation within the condenser. This leads to a lower back-pressure and enables more efficient turbine expansion.

Under the initial condition of 11.88 MW net output, the accumulated NCG concentration was estimated at 2.53%. After optimization, this concentration was reduced to 2.31% due to higher NCG removal through the steam ejector. As a result, the net power production increased by 4.168 kWh. This improvement contributes to a gradual recovery of plant performance toward its installed capacity of 30 MW.

Beyond improving thermal efficiency, the reduction in condenser back-pressure also minimizes mechanical stress on the turbine, potentially extending its operational lifespan. The design, which focuses on achieving optimal pressure ratios and improved entrainment, presents a practical and field-applicable solution that can be replicated in other geothermal ejector units.

3.5 Sensitivity Analysis

The second simulation phase was conducted as a sensitivity analysis to evaluate how the optimized steam ejector design responds to changes in motive steam mass flow rate ($\dot{m}_m$) and suction pressure (P_s), which is assumed equivalent to condenser pressure. The objective was to assess the stability and efficiency of the design under fluctuating operating conditions, as well as to identify potential operating points that maximize performance without altering the physical geometry of the ejector.

Figure 6 shows the effect of varying the motive mass flow rate from 1.46 kg/s to 1.687 kg/s on the

P-ISSN : 2598-1277
E-ISSN : 2621-3966

suction flow rate. Initially, an increase in $\dot{m}_m$ results in a significant rise in suction mass flow ($\dot{m}_s$), but the trend begins to saturate beyond 1.6 kg/s. The optimal point is identified at 1.687 kg/s, corresponding to a suction flow of 0.532 kg/s and an entrainment ratio of 0.32. Beyond this value, further increases in $\dot{m}_m$ provide diminishing returns, indicating the effective mixing limit of the chamber.

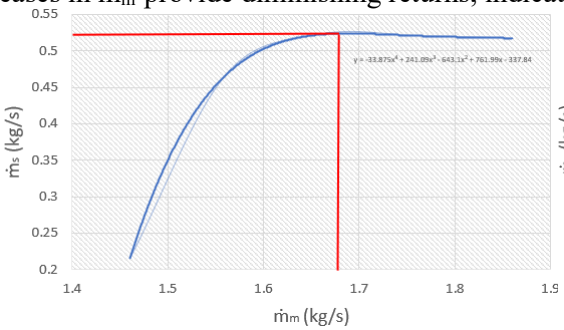

Figure 6. Optimal Process 1

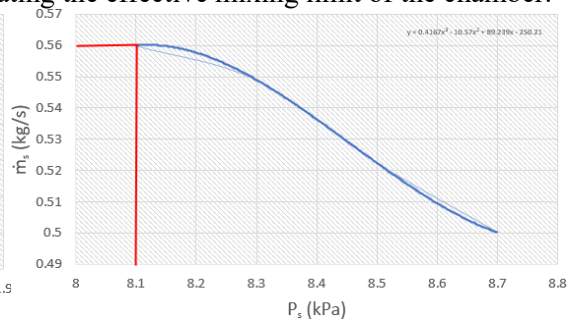

Figure 7. Optimal Process 2

Figure 7 illustrates the influence of suction pressure (P_s) on suction capacity, with a focus on improving condenser vacuum conditions. As P_s decreases from 8.7 kPa to 8.1 kPa, the ejector's suction performance increases significantly. The optimal vacuum point, at P_s 8.1 kPa, yields a suction flow of 0.56 kg/s and an entrainment ratio of 0.34. This emphasizes the importance of improving condenser performance—such as cooling system upgrades or load adjustments—to maintain low outlet pressure and support ejector effectiveness.

Table 3 summarizes the performance of the base design alongside the two optimal operating points. Optimal 1 is achieved by enhancing the condenser vacuum (lower P_s), while Optimal 2 is realized through fine control of the motive mass flow ($\dot{m}_m$). Both strategies improve ejector performance without requiring structural modifications, and also offer practical approaches that can be implemented directly in geothermal field operations.

Table 3. Performance Comparisons

Parameter	Design	Optimal 1	Optimal 2
Ps	8.50 kPa	8.50 kPa	8.10 kPa
ṁm	1.66 kg/s	1.687 kg/s	1.66 kg/s
ṁs	0.52 kg/s	0.532 kg/s	0.56 kg/s
w	0.31	0.32	0.34

These findings indicate that meaningful performance enhancement can be achieved through realistic operational adjustments, without requiring redesign of the ejector's physical structure. This makes the optimized design not only efficient, but also practical and adaptable in real geothermal plant environments.

3.6 Economic Analysis

To evaluate the financial feasibility of the proposed ejector redesign, an economic analysis was conducted, focusing on the investment cost and potential operational benefits. The redesigned mixing chamber requires a total material surface area of 9.96 m², which corresponds to five stainless steel sheets, each measuring 2.97 m² and priced at Rp13,000,000 per sheet [11]. The total material cost is estimated at Rp70,000,000. Additional costs are calculated as percentages of this subtotal 10% for shipping, 30% for installation, and 15% for construction, following standard engineering practices [12]. Operating and maintenance (O&M) costs are assumed to be 2% of the combined cost of materials and installation, as outlined in guidelines from DOE and industrial sources [13].

The total capital investment and O&M amounts to Rp127,984,640. From the performance side, the reduction in NCG fraction from 2.53% to 2.31% increases net generation by 41.68 kWh per day. At a tariff of Rp1,220,69 per kWh [14], and assuming continuous operation for 320 days annually [4], this improvement results in an annual revenue gain of approximately Rp32,876,915 after tax.

P-ISSN : 2598-1277
E-ISSN : 2621-3966

Macroeconomic parameters used in the financial model include a 10% discount rate, 5.50% interest rate, and 1.60% inflation, based on recent economic reports from Bank Indonesia [15].
Table 4 presents the economic results under three conditions: baseline design, Optimal 1 (increased motive flow), and Optimal 2 (enhanced condenser vacuum). Under the base case, the project yields a net present value (NPV) of Rp6,457,037, internal rate of return (IRR) of 11,4%, and payback period of 3 years 10 months 22 days . These values improve further under Optimal 1 and Optimal 2, reaching an NPV of Rp6.457 million, IRR of 11.4%, and a payback period of only 3 years 10 months.

Table 4. Economic Comparisons

Parameter	Design	Optimal 1	Optimal 2
Output	11.884 MWh	11.885 MWh	11.886 MWh
NPV	Rp6,457,036	Rp23.473.671	Rp73,105,521
IRR	11.4%	15.9%	27.1%
PP	3 years 10 months	3 years 5 months	2 years 7 months

These findings show that operational optimization not only enhances technical performance but also significantly improves financial outcomes. The proposed redesign offers a highly feasible investment with very short payback times, making it suitable for replication in similar geothermal units.

4. CONCLUSIONS

The optimization of the steam ejector by reducing the cross-sectional area of the mixing chamber has proven effective in enhancing system performance. The entrainment ratio increased from 0.27 to 0.31, while the NCG suction mass flow improved from 0.45 kg/s to 0.52 kg/s. This confirms the critical role of mixing chamber geometry in improving suction capacity and overall ejector efficiency.
This improvement contributed to an increase in net power generation by 4.168 kWh per day due to a reduction in NCG accumulation within the condenser. As a result, turbine expansion efficiency improved, and the output approached the installed plant capacity of 11.88 MW, with improved condenser vacuum supporting overall system reliability.
From an economic perspective, the proposed design is highly feasible. With an initial investment and O&M cost of approximately Rp127,984,640, the project yields a net present value (NPV) of Rp6,457,036, an internal rate of return (IRR) of 11.4%, and a payback period of 3 years 10 months 22 days. These figures indicate that the optimization is not only technically effective but also financially advantageous, with high profitability and rapid return on investment. The design also offers operational flexibility and can be applied to other geothermal steam ejector systems facing similar performance challenges.

REFERENCES

[1] N. A. Pambudi, “Thermodynamic and economic analysis of combined single and double flash cycle for geothermal power plant,” *Renew. Energy*, vol. 116, pp. 98–107, 2018, doi: 10.1016/j.renene.2017.09.041.
[2] A. Horas, H. R. Silaban, and E. K. Sinaga, “Effect of NCG removal on power output in geothermal power plant,” *J. Rekayasa Proses*, vol. 17, no. 1, pp. 39–44, 2023, doi: 10.14710/jrekpros.17.1.39-44.
[3] H. Pan, Y. Wang, Y. Ma, and Y. Lin, “Numerical investigation of geometric effects on steam ejector performance under unsteady flow,” *Energy*, vol. 193, p. 116745, 2020.

P-ISSN : 2598-1277
E-ISSN : 2621-3966

[4] "Internal Operational Report," 2024.
[5] V. Singhal, S. Sinha, and D. Mahanta, "Design, CFD analysis and performance evaluation of the steam jet ejector," *Int. J. Mech. Eng. Technol.*, vol. 8, no. 7, pp. 451–459, 2017.
[6] H. Zheng, J. Li, H. He, Y. Duan, and Y. Zhang, "Optimization analysis of the mixing chamber and diffuser of ejector based on Fanno flow model," *Energy*, vol. 235, p. 121340, 2021, doi: 10.1016/j.energy.2021.121340.
[7] H. Yan, Q. Liu, D. He, and Y. Cao, "Optimization of two-phase ejector mixing chamber length under varied liquid volume fraction," *Int. J. Refrig.*, vol. 147, pp. 226–236, 2023, doi: 10.1016/j.ijrefrig.2023.01.019.
[8] C. Cai, Q. Chen, and Y. Zhu, "A study of steam ejector performance under various operating conditions," *Appl. Therm. Eng.*, vol. 31, no. 16, pp. 3294–3301, 2011, doi: 10.1016/j.applthermaleng.2011.06.028.
[9] H. El-Dessouky, H. Ettouney, I. Alatiqi, and G. Al-Nuwaibit, "Evaluation of steam jet ejectors," *Chem. Eng. Process.*, vol. 41, no. 6, pp. 551–561, 2002.
[10] ANSYS Inc., "ANSYS Fluent User's Guide, Release 2023 R1," 2023, *Canonsburg, PA, USA*. [Online]. Available: https://www.ansys.com/products/fluids/ansys-fluent
[11] Badan Standarisasi Nasional, *SNI 03-2847-2002: Tata Cara Perhitungan Struktur Beton untuk Bangunan Gedung*. Jakarta: BSN, 2002.
[12] M. S. Peters, K. D. Timmerhaus, and R. E. West, *Plant Design and Economics for Chemical Engineers*, 5th ed. New York: McGraw-Hill, 2003.
[13] United States Department of Energy (DOE), "Geothermal Electricity Technology Evaluation Model (GETEM) Manual," 2013, *Idaho National Laboratory*.
[14] PLN, "Tarif Tenaga Listrik PT PLN (Persero) Tahun 2023," 2023, *Jakarta*. [Online]. Available: https://web.pln.co.id
[15] Bank Indonesia, "Laporan Perekonomian Indonesia 2023," 2024, *Jakarta*. [Online]. Available: https://www.bi.go.id